Nuclear Instruments and Methods in Physics Research B 362 (2015) 103–109

Contents lists available at ScienceDirect

Nuclear Instruments and Methods in Physics Research B

journal homepage: www.elsevier.com/locate/nimb

Investigation on structural aspects of ZnO nano-crystal using radio-active ion beam and PAC

Bichitra Nandi Ganguly [a,*], Sreetama Dutta [a], Soma Roy [a], Jens Röder [b,c], Karl Johnston [b,d], Manfred Martin [c], ISOLDE-Collaboration [b]

[a] Saha Institute of Nuclear Physics, Kolkata 700064, India
[b] Physics Department, ISOLDE/CERN, Geneva, Switzerland
[c] Physical Chemistry, RWTH-Aachen, Aachen, Germany
[d] Experimental Physics, University of the Saarland, Saarbrücken, Germany

ARTICLE INFO

Article history:
Received 7 January 2015
Received in revised form 6 August 2015
Accepted 31 August 2015
Available online 27 September 2015

Keywords:
ZnO nano-crystal
Perturbed angular correlation (PAC)
Radio-active ion beam
Hyperfine interaction

ABSTRACT

Nano-crystalline ZnO has been studied with perturbed angular correlation using ^{111m}Cd, implanted at ISOLDE/CERN and X-ray diffraction using Rietveld analysis. The data show a gradual increase in the crystal size and stress for a sample annealed at 600 °C, and reaching nearly properties of standard ZnO with tempering at 1000 °C. The perturbed angular correlation data show a broad frequency distribution at low annealing temperatures and small particle sizes, whereas at high annealing temperature and larger crystal sizes, results similar to bulk ZnO have been obtained. The ZnO nano-crystalline samples were initially prepared through a wet chemical route, have been examined by Fourier Transform Infrared Spectroscopy (FT-IR) and chemical purity has been confirmed with Energy Dispersive X-ray (EDAX) analysis as well as Transmission Electron Microscopy (TEM).

1. Introduction

ZnO is one of the most versatile wide band gap (3.37 eV) semiconductor materials known for its multifarious applications in technology [1,2]. The aqueous precursor-derived ZnO material is a promising alternative to organic semiconductors and amorphous silicon materials in applications such as transparent thin film transistors at low temperatures [3]. Also, the properties of ZnO transistors depend on its chemical preparation (such as extraction of the precipitate from acidic or basic solutions), drying and sintering processes and also on the traces of impurities imparted to the system [4–6]. Chemical structure analysis suggests that the hydrated zinc cation, the pH of the medium and ligand type play a critical role in aqueous precursor based ZnO-nano-crystalline material.

ZnO is a bio-friendly oxide semiconductor and an inexpensive luminescent material. It is expected to have a wide range of applications in room temperature ultraviolet (UV) lasing [7], biosensors [8], bio-imaging [9], drug delivery [10], piezoelectric transducers [11] and other usages as doped-ceramic compounds [12]. For all such purposes, growth of ZnO nano-size material through a chemical route is a necessity. Most existing preparation techniques rely strongly on ZnO grain manipulation processes while drying and sintering the hydrated ZnO precipitate. Also, the defect structure in the evolution process of nano material is vital as there lies strong evidence that defects have a role to play in ferromagnetic order in such materials and the ferromagnetism coupling may be mediated by carriers [13]. Radiation induced doping [14] and direct radiation effect on the crystal structure can induce static charge localization effects [15], these subtle details in structural analysis play a vital role.

Thus to begin with, a systematic study has been carried out to examine various physical aspects of chemically grown nano-crystalline ZnO. Firstly, the chemical speciation and purity of the as-grown material along with grain growth and crystallinity are checked using several analytical methods like FT-IR spectroscopy, X-ray diffraction method with Rietveld analysis, etc., size and morphology effects through TEM and EDAX have been examined for purity check.

In order to gain detailed information of the growth of nano-crystals of ZnO, the perturbed angular correlation method (PAC) has been found suitable [5,6,16]. This method is employed in order to gain information on doping and its microenvironment in atomic scale [20–22]. But in such cases for the ZnO host, ^{111}In has been used as the probe [5,16–19] which undergoes electron capture (EC) decay, and after-effects of the ^{111}In(EC) → ^{111}Cd process

* Corresponding author. Fax: +91 33 23374637.
E-mail address: bichitra.ganguly@saha.ac.in (B.N. Ganguly).

http://dx.doi.org/10.1016/j.nimb.2015.08.098
0168-583X/

renders the probe into a highly unstable charged state as found in other substrates [23,24]. Also, it is envisaged that some effects could be associated with the valance state of radioactive parent probe nuclei, for example: when the parent nucleus $^{111}In^{3+}$ replaces Zn^{2+}, it may probably induce more defects than $^{111m}Cd^{2+}$. The situation is clearly different than having $^{111m}Cd^{2+}$ as a tracer ion located at isovalent cationic site at the semiconductor oxide material [18,22]. The benefit is the use of a meta-state for PAC, as during the decay, no charge change appears, reducing the effects usually observed by transmutation.

It is thus important to mention that a suitable radioactive dopant ion serving as PAC probe (for example: $^{111m}Cd^{2+}$, by exposure of the ZnO samples to radioactive ion beam at ISOLDE, CERN) becomes a necessity. Further, facilitating the diffusion of the dopant ion into ZnO grains is followed by gradual and controlled annealing steps under vacuum. An improvement of grain size consistency by controlling the formation of ultrafine grains and prevention of abnormal grain growth could yield a better result for fabricating nano-material for a device related purpose. Although we find ZnO nano-material has been studied in various ways, but a systematic monitoring of the structural distribution in the presence of a dopant like Cd^{2+} through PAC [22] at trace level in the host medium along with sintering processes are sparse. In this work, we have purportedly used $^{111m}Cd^{2+}$ such that its direct route to stable state will not alter any other characteristics of the medium except the electric field gradient (EFG) tensor, which is the observable parameter from PAC measurement. Such a parameter is strongly dependent on the distribution of the electronic charge density around the site where the radioactive probe atom has been hosted in the lattice.

In this article, we develop a meaningful comparison of the changes that have been observed for pure ZnO nano-crystal, starting from the defect structure caused due to radioactive ion beam irradiation by using the technique: PAC measurements, after subjecting the material through a few sequential and controlled vacuum annealing steps. The same is compared with X-ray diffractions studies and Rietveld analysis, for the structural aspects of ZnO nano-crystalline material.

2. Experimental

2.1. Chemical synthesis of pure zinc oxide

ZnO nano particles were prepared by the wet-chemical route from zinc acetate, $Zn(CH_3COO)_2{\cdot}2H_2O$ (extra pure AR grade material, from SRL, India). The desired weight of zinc acetate was dissolved in triple distilled water (TDW) and a (1:1/vol) ammonia solution (Merck India) was added to this solution drop by drop, maintaining a pH $\approx$ 7.5. Initially zinc is precipitated as zinc hydroxide. After centrifugation, the precipitate was collected and re-dispersed into TDW to remove excess ions. Finally, the precipitate was recollected and dried at 100 °C for 12 h in vacuum oven and sintered at different temperatures (200, 600 and 1000 °C for 30 min) under vacuum to evolve ZnO nano-crystallites. These ZnO nano-grains were characterized by Fourier Transmission Infrared (FT-IR) Spectroscopy [25] (as pellets in KBr, without moisture) using a Perkin Elmer FTIR system, Spectrum 100) in the range of 400–4500 cm^{-1}, with a resolution of 0.4 cm^{-1}. The results are shown in Fig. 1 and Table 1.

2.2. Electron microscopic studies

For the elemental purity check of the ZnO samples, Energy Dispersive X-ray analysis (EDAX/SEM) and scanning microscopic analysis of the grain surface was performed using Quanta FEG-200, FEi Company USA. As prepared ZnO sample sintered at 200 °C, has been dispersed in pure water then TEM examination was performed after placing a drop of the same on the carbon coated grid and dried under vacuum. Measurements were done with (Tecnai S-twin, FEI) using an accelerating voltage of 200 kV, having a resolution of ≈1 Å. The results of such analysis are shown in Fig. 2.

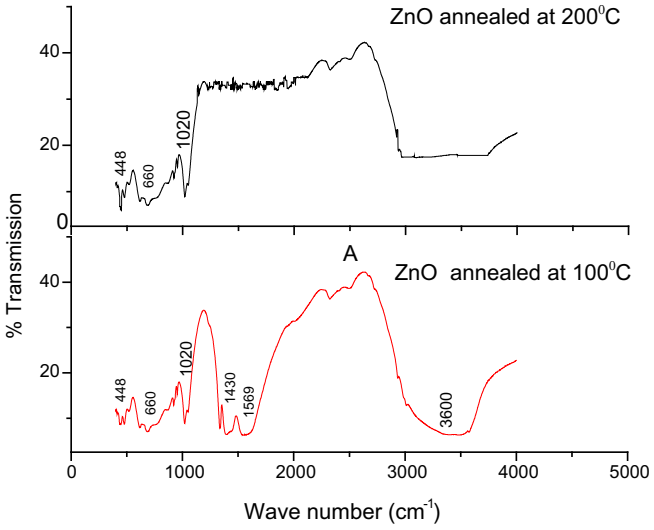

Fig. 1. FT-IR spectrum representing the characteristic frequencies of ZnO material synthesized from aqueous route and dried in vacuum oven at 100 °C for 12 h and then dried to 200 °C.

Table 1
IR spectroscopic group frequencies [25] for the prepared pure ZnO nano-crystalline sample, dried at 100 °C and compared to that after drying to 200 °C (refer to Fig. 1).

Absorption wave number cm^{-1}	Functional group frequencies
~500, 525–560	Zn—O stretching
~1020	H—O—H bending
1430, 1570	—C=O stretching
~3500 and greater	—OH stretching

2.3. Characterization with X-ray powder diffraction measurements

The phase structures of the samples were identified by X-ray diffraction, Rigaku TTRAX3 diffractometer with CuK$\alpha_{1,2}$ radiation (λ = 1.541 Å and 1.5444 Å) has been used. The data have been collected in the range (2θ) 10–100° with a step size of 0.02°. Si has been used as an external standard to deconvolute the contribution of instrumental broadening [26]. The measured XRD pattern is shown in Fig. 3a.

Additionally, Rietveld refinement analysis was performed with GSAS [27,28], calibrating the instrumental parameters with a standard Si measurement. The results are shown in Fig. 3b. In all the fits, instrumental parameters were kept constant.

From Thompson–Cox–Hastings pseudo-Voigt function (TCH) of the Lorentzian and Gaussian term, size and strain parameters can be retrieved directly from GSAS profile parameters [29], using Lorentzian TCH term with parameters GX and GY:

$$\Gamma_L = \frac{GX}{\cos\theta} + GY\tan\theta \quad (1)$$

For the Williamson-Hall analysis, the integral breath (β) holds with D_v as the volume weighted average, ε_{str} the strain and λ as the wavelength:

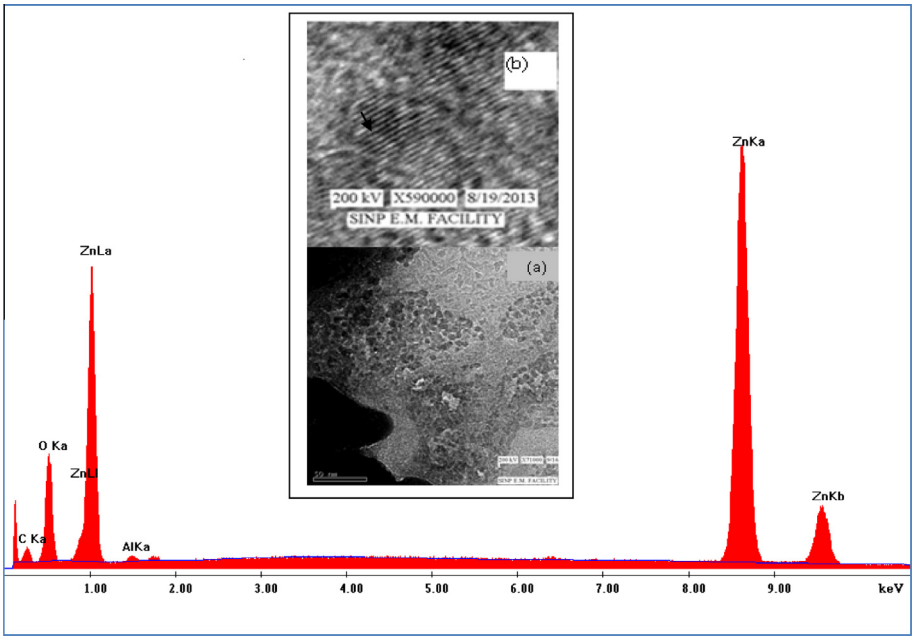

Fig. 2. EDAX data: a purity check of the ZnO sample as synthesized through sol–gel chemical route, inset shows the ZnO nano particles with fringed structure of the crystalline sample from TEM picture.

$$\{\beta_{obs} - \beta_{inst}\} = \frac{\lambda}{(D_v \cos\theta)} + 4\varepsilon_{str}(\tan\theta) \quad (2)$$

A correction of the FWHM to integral breath and correcting GSAS centi-degrees, size and strain can be calculated by:

$$D_v = 36000\frac{\lambda}{\pi^2 GX} \quad (3)$$

$$\varepsilon_{str} = \frac{\pi^2(GY - GY_{inst})}{144000} \quad (4)$$

Gaussian TCH term with parameters GU and GP (GV and GP can be considered as instrumental constants):

$$\Gamma_G = GU\ \tan^2\theta + GV\ \tan\theta + GW + \frac{GP}{\cos\theta} \quad (5)$$

Williamson-Hall analysis:

$$\{\beta_{obs}^2 - \beta_{inst}^2\} = \frac{\lambda^2}{\{(D_v)^2\cos^2\theta\}} + 16(\varepsilon_{str})^2\tan^2\theta \quad (6)$$

Applying the same corrections as for the Lorentzian part results in:

$$D_v = 18000\frac{\lambda}{\mathrm{sqrt}(2\pi^3 GP)} \quad (7)$$

$$\varepsilon_{str} = \frac{\mathrm{sqrt}\{2\pi^3(GU - GU_{inst})\}}{72000} \quad (8)$$

The volume weighted average D_v can be converted into the diameter of spheres with identical size: $d = 4/3D_v$ (see Tables 2 and 3).

2.4. Local structure investigation with perturbed angular correlation using radioactive ion beam of ^{111m}Cd

The time differential perturbed angular correlation technique is based on the modulation of angular correlation of the successive radiations emitted during a nuclear decay cascade due to hyperfine interactions between the electromagnetic moments of the intermediate nuclear level with its immediate neighboring electronic environment. Suitable isotopes for standard PAC have an intermediate level (sensitive level) which has a half-life between 10 and 1000 ns (see Fig. 4), while the half-life of the parent isotope is sufficiently long lived to provide a measurement. ^{111}In with a 2.8 days half-life and simple cascade is one of the most and widely-used PAC probes. However, the so-called *after effects*, resulting from the change of electronic charge state from $^{111}In^{3+}$ to $^{111}Cd^{2+}$, can be problematic especially in semiconductors [30]. In order to minimize these effects, the $^{111m}Cd^{2+}$ radioactive ion is more suitable as it does not undergo any such transmutation. However, its short half life of 48 min restricts its availability to on-site measurements at a facility such as ISOLDE at CERN.

A PAC machine consists of a setup of usually four or six detectors which measure the time difference between the γ_1 and γ_2-ray as shown in Fig. 4, from which the radioactive decay curve of the intermediate level of ^{111m}Cd with a life time of ≈84.5 ns has been obtained. Due to the anisotropy of the emitted radiation, ripples on the decay curve become visible when electric quadrupole or/and magnetic dipole interaction, e.g. electric field gradient (EFG) or local magnetic fields in magnetic materials, are non-zero as shown in Fig. 4 (see in the middle). The counting rate ratio, $R(t)$, is obtained from the coincidence data by:

$$R(t) = 2\frac{N^{180^\circ}(t) - N^{90^\circ}(t)}{N^{180^\circ}(t) + 2N^{90^\circ}(t)} \quad (9)$$

The counting rate ratio can be described in practical use by [31]:

$$R(t) \approx A_{22}^{eff}\sum_i f_i G_{22}^i(t) \quad (10)$$

where A_{22}^{eff} is the effective anisotropy, f the fraction per site i and G_{22} the perturbation factor. For quadrupole interaction, including the finite time resolution here in the last term, the following expression was used for fitting the data:

$$G_{22}^i(t) = s_{20}^i(\eta_i) + \sum_{j=1}^{3} s_{2j}^i(\eta_i)\cos(\omega_j^i t)e^{-\frac{\omega_j^i \delta_i t}{\nu_{Q_i}}} e^{-\frac{(\omega_j^i \tau_r)^2}{16\ln 2}} \quad (11)$$

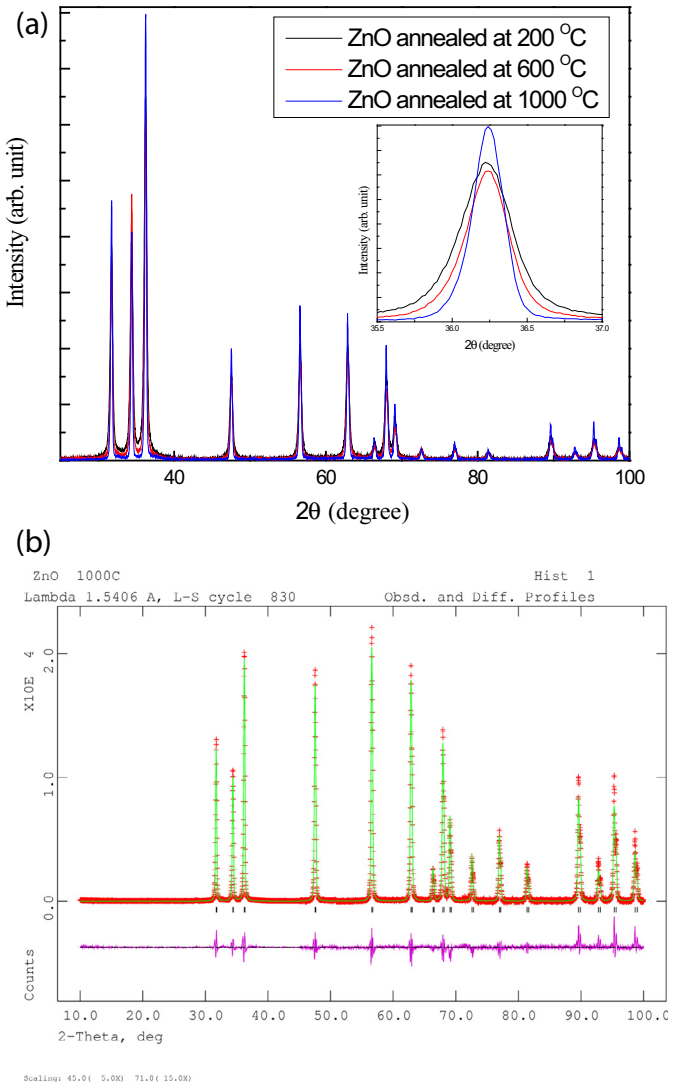

Fig. 3. (a) X-ray diffraction pattern (raw data as obtained) ZnO-nano crystalline grains at different sintering temperatures. (b) Rietveld fit with GSAS. Graph is scaled twice.

In this expression, v_Q is the quadrupole interaction constant with δ its distribution, ω is the quadrupole circular frequency and τ is the instrumental time resolution. The term:

$$d_n(\omega_i, \tau_r) = e^{-\frac{(\omega_j^i \tau_r)^2}{16 \ln 2}} \quad (12)$$

takes into account the Gaussian and Lorentzian time resolution broadening [32,33]. More detailed description of the PAC method can be found at [31,34–36].

Perturbed Angular Correlation (PAC) spectroscopy was performed in order to study the local structure in polycrystalline nano-ZnO. ^{111m}Cd as PAC probe was implanted into cold pressed pellets of the previously prepared material. Room temperature implantations were performed at ISOLDE/CERN [37] at 30 keV. $^{111m}Cd^+$ was produced following irradiation of a molten Sn target by 1.4 GeV protons, which were subsequently plasma ionized and mass separated. A typical irradiation dose was about 3×10^{13} ions per sample.

PAC measurements were performed at room temperature (RT) using two Digital Time Differential PAC machines (DTDPAC) [38,39] with four BaF_2 detectors resulting in 12 single spectra of 90° and 180° per measurement. All the detected γ-rays were saved as time and energy values on the DTDPAC machine's hard disks. Due to the short half-life of the probe, energy windows shifted slightly with the rather fast decrease of the radioactivity. Therefore the recorded data were reprocessed by separating the data into several parts, the optimal energy windows were determined for each part and the results of all parts were finally merged together. The data were analyzed with XFIT program, using the XPAC for the same program [40].

3. Result and discussion

3.1. FT-IR and EDAX study

ZnO samples prepared by aqueous sol–gel technique were dried under vacuum at 100 °C over night, and the characteristic FT-IR frequencies were checked as shown in Fig. 1 and Table 1 for any residual organic groups. These data represent the as-prepared ZnO material. Some residual acetate groups (C═O) could be detected. Presence of moisture is also detected; this could be dependent on the ambient condition. It was considered as the precursor material for ZnO, which was sintered later to proceed for evolution of pure and dried material of ZnO. The elemental purity of ZnO was checked with the help of EDAX spectrum as shown in Fig. 2. From TEM results of pure ZnO samples (dried at 200 °C was used), the fringe structure of ZnO sample showed crystallinity of the material (as shown by the arrow). The mean size as estimated from the TEM image has been about ≈10 nm (average size as measured with the size bar shown in the figure) and clearly indicates that the initially annealed ZnO nano-particles are crystalline with a wurtzite structure [41]. No other impurities were observed.

3.2. X-ray diffraction (XRD) study

The as-dried precipitate of ZnO material (at 100 °C) can be considered as a precursor of the ZnO material without the typical ZnO phase, but mainly zinc acetate phase and an unknown phase. Further annealing of this sample stage by stage from (200–1000 °C) or precisely at 200, 600 and 1000 °C, pure ZnO

Table 3
The unit cell parameters after sintering at 1000 °C as per Rietveld refinement analysis.

Spacegroup	a (Å)	c (Å)	α, β (°)	γ (°)
P 63 m c	3.2499	5.2056	90	120
Atom/charge	x	y	z	100 * Uiso
Zn + 2	0.3333	0.6666	0	2.917
O − 2	0.3333	0.6666	0.3759	3.517

Table 2
Lattice parameters at different sintering temperatures as per the Rietveld GSAS refinement analysis, Scherrer constant $K = 1$.

Temperature (°C)	a (Å)	c (Å)	Texture Index (GSAS)	Strain (%)	Size (nm) (diameter of spherical particles)
200	3.2500	5.2070	1.078	Negligible	26
600	3.2496	5.2057	1.147	0.0856	46
1000	3.2499	5.2056	1.021	0.0188	76

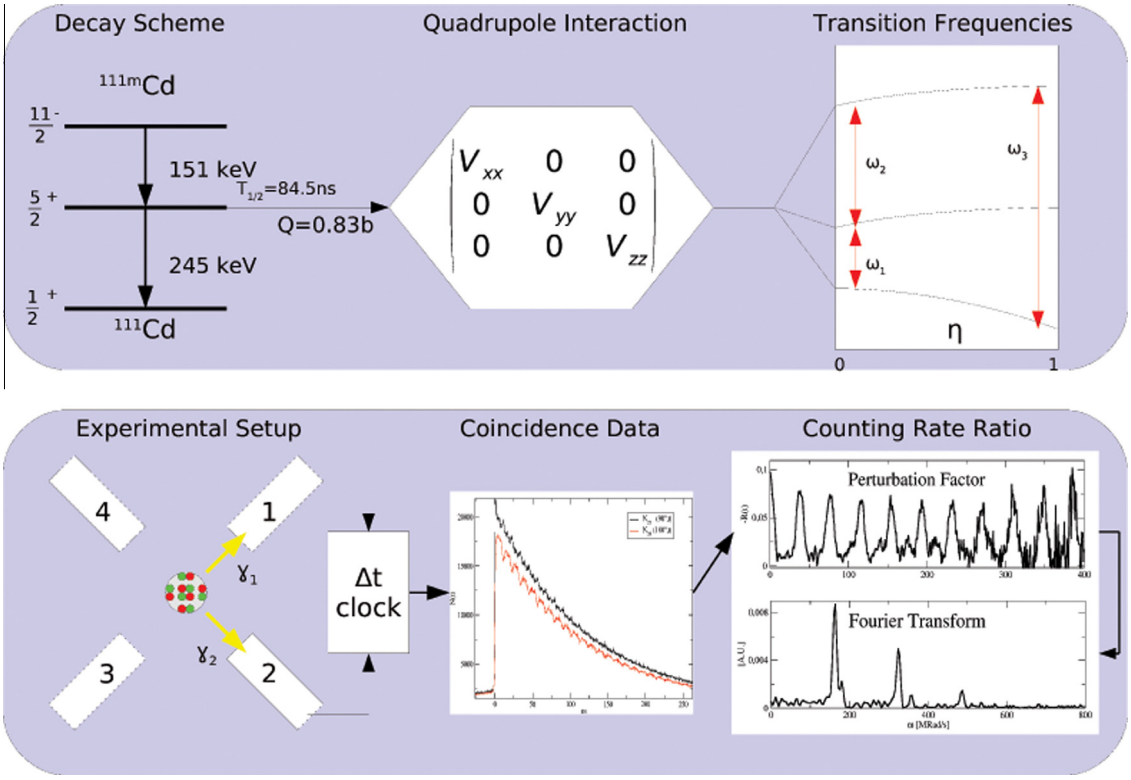

Fig. 4. Decay scheme of ^{111m}**Cd**$_{48}$, IT, $\mathbf{T_{1/2}}$ **= 48.54 m**, isomeric level with $5/2^+$ spin where EFG tensor interacts with nuclear quadrupole moment *Q*, an illustration of the typical PAC measurement.

structure was produced, no characteristic peaks from intermediates such as $Zn(OH)_2$ could be detected in the samples. XRD results shown in Fig. 3a give us the characteristic diffraction pattern of the crystallites under the particular configuration, through the Bragg angles. The appearance of characteristic diffraction peaks for a pure ZnO sample corresponding to (100), (002), (101), (102), (110), (103) and (112) planes is in good agreement with the standard XRD peaks of crystalline bulk ZnO with hexagonal wurtzite structure [JCPDS card No. 36-1451, $a = 3.2501$ Å, $c = 5.2071$ Å, space group: P63mc (186)]. The gradual changes of the FWHM of characteristic peak (002) is shown as an inset to show the refinement of evolved structure, at 1000 °C, the best result is obvious from the spectrum.

The Rietveld refinement analysis was performed using GSAS. For performing the Rietveld fitting, the instrumental parameters were determined by using a standard Si sample. (Fitted data according to GSAS labeling were LX, LY, shft, ptec, lattice parameters, fractional coordinates and Uiso as well as spherical harmonics, preferred orientation with 6th order.) Lattice parameters are shown at different sintering temperatures in Table 2 and the unit cell parameters after sintering at 1000 °C in Table 3.

While fitting these nano-crystallite parameters, an unusual peak shape was observed which could not be fully adjusted by keeping the instrumental parameters fixed. This may indicate an irregular structure or larger variation in crystallite size. The fit could be improved by adding a Gaussian component by parameters GU and GP, see Fig. 3b for the sample sintered at 1000 °C. (In General, the Lorentzian term of the Thompson–Cox–Hastings pseudo-Voigt function mainly fits sufficiently well crystallized material with Bragg–Brentano X-ray powder diffractometers, so that Gaussian terms (GU, GP) are rarely used.)

From Thompson–Cox–Hastings pseudo-Voigt function (TCH) of the Lorentzian and Gaussian term, size and strain parameters can be retrieved directly from GSAS profile parameters. The analysis of the powder, which was sintered at different temperatures, has been summarized in Table 2. The crystalline size is assumed by a model for spherical particles of the same size. It increases steadily with increasing sintering temperature, while the lattice parameters stay almost unchanged. As the sintering temperature gradually increases and the crystal size increases, the lattice strain is found to be at maximum at 600 °C. Lattice strain arises generally due to vacancies, crystal imperfection, dislocations sinter stress, stacking faults etc., which in case of nano-materials can also be induced by surface tension effects. Also, the texture is found to be strongest at 600 °C sintered sample, where also stain is the highest as well.

3.3. Perturbed γ–γ angular correlation measurements

In order to understand the changes in the local structure and the material properties induced due to subsequent annealing of ZnO, perturbed angular correlation spectroscopy (PAC) was performed with the probe $^{111m}Cd^{2+}$ and results are shown in Figs. 5a, b, c.

The PAC experimental runs have been performed at room temperature, at first, without annealing ZnO sample (precursor material) and then after subsequent annealing of the ZnO samples at temperatures 600 °C, and 1000 °C respectively after implantation of $^{111m}Cd^{2+}$ for 30 min to anneal implantation defects. However, the high annealing temperatures for the same time duration are sufficient to bring in change in nano materials in terms of increase in crystal size and their properties as well. At room temperature, the $^{111m}Cd^{2+}$ doped precursor ZnO sample shows no frequencies corresponding to standard ZnO, but a wide distribution of frequencies can be seen in Fig. 5a. The sample sintered at 600 °C shows a known frequency from $\nu_Q \approx 30$ Hz, (can be compared with earlier results [5]), with a wide distribution of about 4 ± 12 MHz and $\eta \approx 0.5 \pm 0.5$, while the material sintered at 1000 °C shows $\nu_Q \approx 31$ Hz and $\eta \approx 0.1$. Due to low statistics at the 600 °C

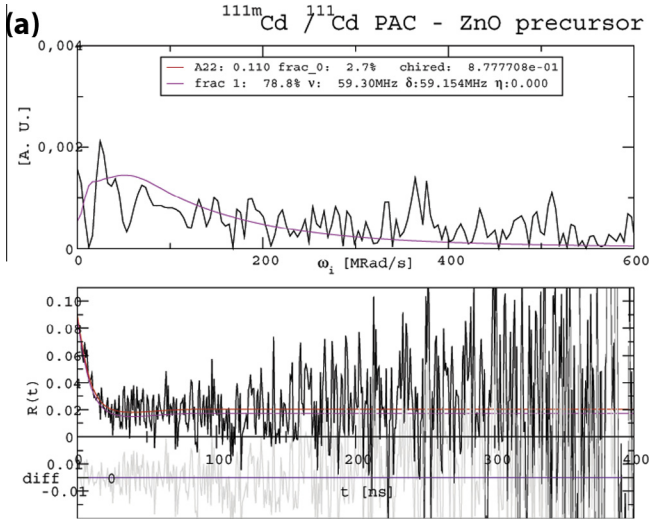

Fig. 5a. PAC measurements after implantation of $^{111m}Cd^{2+}$ at RT in ISOLDE experiment, without annealing, showing the experimental $R(t)$ spectrum and the hyperfine interactions.

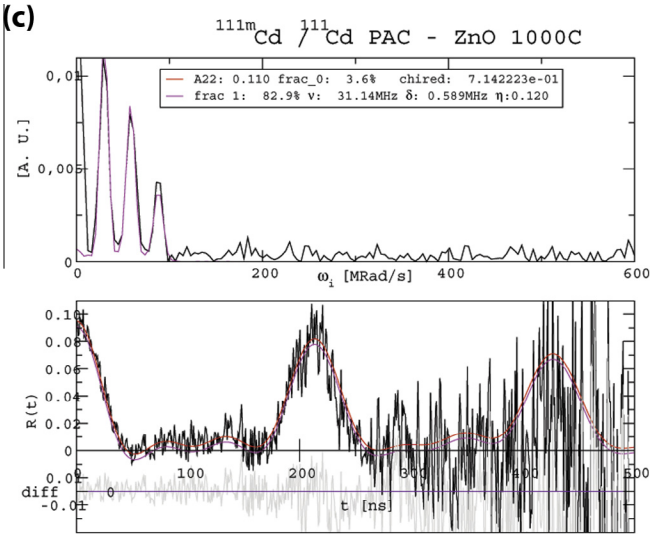

Fig. 5c. ZnO nano-crystalline material was doped with $^{111m}Cd^{2+}$ in ISOLDE experiment and annealed at 1000 °C, measured in PAC set up. The experimental $R(t)$ spectrum shows well defined hyperfine interaction and the Fourier transforms of the hyperfine parameters are also represented (top). The data shown in the legend are from the fit program. Error corrected data are in Table 4.

tempered sample, errors are considerably high, reducing the significance of the data. However it is clearly visible that the amplitude at ≈210 ns is nearly absent in this sample as compared to the 1000 °C sample. As the A_{22} is a nucleus property and in a measurement is decreased by the detector size and distance, it is machine related observed A_{eff} is at around 0.1. As reference on this, the observed fraction of the sample at 600 °C is significantly lower with only 50% than compared to the sample at 1000 °C with 83%, which indicates that many probes of the 600 °C tempered sample are on non contributing locations. This may indicate a highly distorted environment and can be probably caused by the higher shell quantity considering the core–shell model of small particles [5,18]. Comparing the three measurements, the development indicates a steady growth of crystallinity, in agreement with the X-ray diffraction data in case of the growth of crystal size, and can be compared with results of reference [22]. It is possible to assume also that there could be an incomplete radiation/implantation damage

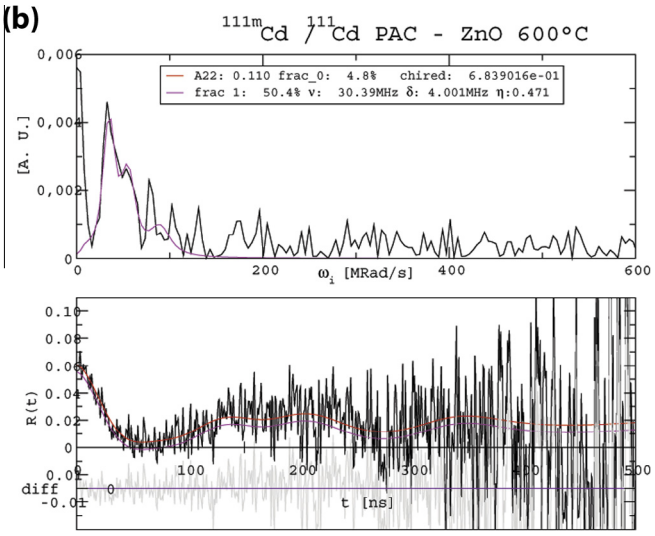

Fig. 5b. PAC measurements after doping $^{111m}Cd^{2+}$ in ISOLDE experiment and after annealing at 600 °C, showing the experimental $R(t)$ spectrum and the hyperfine interactions. The data shown in the legend are from the fit program. Error corrected data are in Table 4.

recovery of the material structure. However, the recrystallization of nano-ZnO is probably more significant here. The asymmetry parameter (η) is also larger at 600 °C, but the error is in the same order, so that its significance with the current statistics of the measurement is not high enough. However, it would indicate a highly distorted environment and the same could be due to random distribution of static crystal defects. The observed differences overlap well with the observations of the X-ray data and their Rietveld analysis. The deviation from normal peak profile and as well the increased stress at the 600 °C indicate that the nano-ZnO sample undergoes changes during the recrystallization (through vacuum annealing stages), which the data of both the methods (namely X-ray diffraction analysis as well as PAC) indicate. Barbosa et al. [22] observed a second frequency in thin film ZnO at 800 °C annealing temperature. It is interesting that our data at 600 °C near this temperature also show alterations from the normal bulk properties. But it needs to be mentioned that our data were measured at room temperature and that nano materials are mainly from low crystalline quality where this frequency might be difficult to observe. Nevertheless, both data indicate that there might be an effect worth to be further investigated. The PAC results are shown in Table 4.

As the density functional theory calculations [5] of the lattice sites, the EFG have been performed with good agreement of Cd^{2+} impurities into ZnO host nano-structure, through the measurements. This confirms well with the expectations for incorporation of Cd^{2+} in ZnO as both the metals are from the same IIB group of elements, having similar crystal radii (see preference of crystal radii over ionic radii in crystals [42]) with Cd^{2+} in tetragonal coordination with r_{Cd+2} = 0.97 Å and for Zn^{2+} in equivalent environment

Table 4
Hyperfine interaction parameters of ZnO derived from the PAC in the ZnO samples showing profound effect on annealing temperature (refer to Fig. 5a, b, c).

T (°C) (annealing temperature)	Fraction (%)	ν_Q (MHz)	δ (MHz)	η
RT (precursor)	78.8 ± 78	59.3 ± 200	59.2 ± 300	0 ± 0.2
600	50.4 ± 50	30.4 ± 12	4.00 ± 12	0.47 ± 0.5
1000	82.9 ± 22	31.2 ± 2	0.59 ± 0.5	0.12 ± 0.3

with r_{Zn+2} = 0.74 Å. As Cd^{2+} is larger than Zn^{2+}, the local structure may be slightly distorted, which may cause a larger effect in highly distorted material, where restoring forces are smaller. The final sintering at high temperatures of 1000 °C transforms the material in normal bulk ZnO.

The performed measurements suggest that the preparation of nano-ZnO by the wet chemical method provides different materials properties (surface defects are common features in nano-size particles, see Tables 2 and 3) which are possibly scalable with sintering conditions. But due to radioactive ion beam implantation method, there are damages caused which are gradually recovered through sequential sintering processes.

4. Conclusion

ZnO material prepared through wet chemical route, sintered at 200 °C already forms ZnO with small crystallite size ⩽26 nm (TEM examination shows smaller size), but has been continuously growing with further tempering at higher temperature.

Perturbed angular correlation using the ^{111m}Cd probe confirmed the results with previous works and shows that the material at lower sintering temperatures possesses a higher order distorted local structure, due to stress in the nano-material as shown from the X-ray diffraction studies and due to higher ratio of shells in the core–shell model, which also results in a disordered material. The ZnO structure is partially recovered after sintering at 1000 °C, but still shows effects of nano-material properties with crystal sizes below the 100 nm regime. PAC data of the sample at 1000 °C shows analyzed results that are comparable to bulk material. The result of the sample tempered at 600 °C, is interesting since it indicates increased stress from Rietveld analysis and a defect rich environment from PAC data.

Structurally different, evolving nano-ZnO crystalline grains could be further useful for future study of semi-conductor application in requirements like thin film transistors, optoelectronic devices and development of flexible electronics etc. with new properties.

References

[1] Zhong Lin Wang, J. Phys.: Condens. Matter 16 (2004) R829–R858.
[2] K. Nomura, H. Ota, A. Tagaki, T. Kamiya, M. Hirano, H. Hosono, Nature 432 (2004) 488–492.
[3] H.E.A. Huitema, G.H. Gelinck, J.B.P.H. van der Putten, K.E. Kuijk, C.M. Hart, E. Cantatore, P.T. Herwig, J.M.J.M. van Breemen, D.M. de Leeuw, Nature 414 (2001) 599.
[4] Taehwan Jun, Yangho Jung, Keunkyu Song, Jooho Moon, Appl. Mater. Interfaces 3 (2011) 774–781.
[5] Emiliano L. Munõz, Marcio E. Mercurio, Moacir R. Cordeiro, Luciano F.D. Pereira, Artur W. Carbonari, Mario Rentería, Physica B 407 (2012) 3121–3124.
[6] S.B. Rana, P. Singh, A.K. Sharma, A.W. Carbonari, R. Dogra, J. Optoelectron. Adv. Mater. 12 (2010) 257–261.
[7] Z.K. Tang, G.K.L. Wong, P. Yu, M. Kawasaki, A. Ohtomo, H. Koinuma, Y. Segawa, Appl. Phys. Lett. 72 (1998) 3270–3272.
[8] Z. Zhao, W. Lei, X. Zhang, B. Wang, H. Jiang, Sensors 10 (2010) 1216–1231.
[9] K. Senthilkumar, O. Senthilkumar, K. Yamauchi, M. Sato, S. Morito, T. Ohba, M. Nakamura, Y. Fujita, Phys. Status Solidi B 246 (2009) 885–888.
[10] Y. Wang, L. Chen, Nanomed. Nanotechnol. Biol. Med. 7 (2011) 385–402.
[11] D.C. Oertel, M.G. Bawendi, A.C. Arango, V. Bulovic, Appl. Phys. Lett. 87 (2005) 213505–213507.
[12] D.R. Clarke, J. Am. Ceram. Soc. 82 (1999) 485–502.
[13] M. Khalid, M. Ziese, A. Setzer, P. Esquinazi, M. Lorenz, H. Hochmuth, M. Grundmann, D. Spemann, T. Butz, G. Brauer, W. Anwand, G. Fischer, W.A. Adegabo, W. Hergert, A. Ernst, Phys. Rev. B 80 (2009) 035331–035335.
[14] T. Mookherjee, Phys. Status Solidi (a) 13 (1972) 293–301.
[15] S. Brunner, W. Puff, P. Mascher, A.G. Balogh, MRS Proc. 540 (1998) 207, http://dx.doi.org/10.1557/PROC-540-207.
[16] M.E. Mercurio, A.W. Carbonari, M.R. Cordeiro, R.N. Saxena, L.Z.D. Agostino, J. Magn. Magn. Mater. 322 (2010) 1195–1197.
[17] Th. Agne, Z. Guan, X.M. Li, H. Wolf, Th. Wichert, Phys. Status Solidi (B) 229 (2002) 819–823.
[18] T. Agne, M. Deicher, V. Koteski, H.E. Mahnke, H. Wolf, T. Wichert, Hyperfine Interact. 159 (2004) 55–61.
[19] Th. Agne, Z. Guan, X.M. Li, H. Wolfand, Th. Wichert, H. Natter, R. Helpenmann, Appl. Phys. Lett. 83 (2003) 1204–1206.
[20] M.A. Nagl, M.B. Barbosa, U. Vetter, J.G. Correia, H.C. Hofsäss, Nucl. Instr. Meth. Phys. Res. A 726 (2013) 17–30.
[21] R. Dogra, A.P. Byrne, L.L. Araujo, M.C. Ridgway, Nucl. Instr. Meth. Phys. Res. B 257 (2007) 355–358.
[22] M.B. Barbosa, J.N. Gonçalves, A. Redondo-Cubero, S.M.C. Miranda, R. Simon, P. Kessler, M. Brandt, F. Henneberger, E. Nogales, B. Méndez, K. Johnston, E. Alves, R. Vianden, J.P. Araújo, K. Lorenzand, J.G. Correia, Phys. Status Solidi B 250 (2013) 801–808.
[23] A.G. Bibiloni, C.P. Massolo, J. Desimoni, L.A. Mendoza-Zélis, F.H. Sánchez, A.F. Pasquevich, L. Damonte, A.R. López-García, Phys. Rev. B 32 (1985) 2393.
[24] D. Lupascu, S. Habenicht, K.-P. Lieb, M. Neubauer, M. Uhrmacher, T. Wenzel, Phys. Rev. B 54 (1996) 871–883.
[25] L.J. Bellamy. Infrared Spectra of Complex Molecules, Methuen, London, 1959.
[26] B.D. Cullity, S.R. Stock, Elements of X-ray Diffraction, Prentice-Hall, Englewood Cliffs, New Jersey, 2001.
[27] A.C. Larson, R.B. Von Dreele, Los Alamos National Laboratory Report LAUR (2000) 86–748.
[28] B.H. Toby, J. Appl. Crystallogr. 34 (2001) 210–213.
[29] P. Karen, P.M. Woodward, J. Solid State Chem. 141 (1998) 78–88.
[30] M. Uhrmacher, Phys. B 389 (2007) 58–66.
[31] H. Frauenfelder, in: K. Siegbahn (Ed.), R.M. Steffen, Alpha-, Beta-, Gamma-Ray Spectroscopy, vol. 2, North Holland, Amsterdam, 1965, pp. 997 (Chapter XIX).
[32] A. Bartos, M. Uhrmacher, Phys. Rev. B 48 (1993) 7478–7485.
[33] J.D. Rogers, A. Vasquez, Nucl. Instr. Meth. 130 (1975) 539–541.
[34] A. Weidinger, M. Deicher, Hyperfine Interact. 10 (1981) 717–720.
[35] J. Röder, K.D. Becker, in: R. Schäfer, P.C. Schmidt (Eds.), Methods in Physical Chemistry, Wiley-VCH, Weinheim, 2012.
[36] E.N. Kaufmann, R.J. Vianden, Rev. Mod. Phys. 51 (1979) 161–214.
[37] E. Kugler, Hyperfine Interact. 129 (2000) 23–42.
[38] C. Herden, J. Röder, J.A. Gardner, K.D. Becker, Nucl. Instr. Meth. Phys. Res., Sect. A 594 (2008) 155–161.
[39] J. Röder, C. Herden, J.A. Gardner, K.D. Becker, M. Uhrmacher, H. Hofsäss, Hyperfine Interact. 181 (2008) 131–139.
[40] J. Röder, PAC Spektroskopie an Ruddlesden-Popper Phasenundmethodische Entwicklungen zur Digitalen PAC-Spektroskopie, Sierke Verlag, 2009.
[41] Sreetama Dutta, Bichitra Nandi Ganguly, J. Nanobiotechnol. 10 (2012) 29–38.
[42] R.D. Shannon, Acta Crystallogr. A 32 (1976) 751–767.